

# GEOGRAPHIC AND SEASONAL INFLUENCES ON OPTICAL FOLLOWUP OF GRAVITATIONAL WAVE EVENTS

VARUN SRIVASTAVA<sup>1,2</sup>, VARUN BHALERAO<sup>3</sup>, ARAVIND P. RAVI<sup>4,5</sup>, ARCHISMAN GHOSH<sup>5,6</sup>, SUKANTA BOSE<sup>3,7</sup>

<sup>1</sup>Indian Institute of Science Education and Research Pune, Dr. Homi Bhabha Road, Pashan, Pune 411008, India

<sup>2</sup>[varun.srivastava@students.iiserpune.ac.in](mailto:varun.srivastava@students.iiserpune.ac.in)

<sup>3</sup>Inter-University Centre for Astronomy and Astrophysics, Post Bag 4, Ganeshkhind, Pune 411 007, India

<sup>4</sup>Indian Institute of Science Education and Research Kolkata, Mohanpur, West Bengal 741252, India

<sup>5</sup>International Centre for Theoretical Sciences, Tata Institute of Fundamental Research, Survey No. 151, Shivakote, Hesaraghatta Hobli, Bengaluru North 560089, India

<sup>6</sup>Nikhef – National Institute for Subatomic Physics, Science Park 105, 1098 XG Amsterdam, The Netherlands

<sup>7</sup>Department of Physics & Astronomy, Washington State University, 1245 Webster, Pullman, WA 99164-2814, U.S.A

## ABSTRACT

We investigate the effects of observatory locations on the probability of discovering optical/infrared counterparts of gravitational wave sources. We show that for the LIGO–Virgo network, the odds of discovering optical/infrared (OIR) counterparts show some latitude dependence, but weak or no longitudinal dependence. A stronger effect is seen to arise from the timing of LIGO/Virgo observing runs, with northern OIR observatories having better chances of finding the counterparts in northern winters. Assuming identical technical capabilities, the tentative mid-2017 three-detector network observing favors southern OIR observatories for discovery of EM counterparts.

## 1. INTRODUCTION

The detection of gravitational waves (GW) by LIGO (Abbott et al. 2016b; The LIGO Scientific Collaboration & the Virgo Collaboration 2016) marks the beginning of the era of gravitational wave astronomy. Continued improvements in the sensitivity of GW detectors will increase the frequency of detections, enabling detailed study of a variety of sources and source populations.

An key step in the study of GW sources is the detection of electromagnetic (EM) counterparts. While GW signals carry information about physical and geometric properties of the source, study of EM counterparts will yield complementary information necessary to complete our astrophysical understanding of the source (Nissanke et al. 2013; Singer et al. 2014). Several groups around the world partook in efforts to follow-up the first gravitational wave detections (Abbott et al. 2016a,c), leading to the discovery of a candidate gamma ray signal potentially associated with binary black hole merger event GW150914 (Connaughton et al. 2016). There is greater potential for the existence of EM counterparts of GW sources like binary neutron star mergers or supernovae, and several groups will take part in followup activities for future gravitational wave triggers<sup>1</sup>.

The localization of a GW source by a pair of gravitational wave detectors depends on source parameters and signal strength, and is rather coarse: the 90% credible regions of the sky localization often span hundreds of square degrees (Singer et al. 2014; The LIGO Scientific Collaboration & the Virgo Collaboration 2016). Imaging such large sky areas to find specific transient counterparts poses formidable challenges (cf. Singer et al. 2015). Various aspects of this challenge have been examined in detail, including theoretical modeling of light curves of GW events (Tanaka & Hotokezaka 2013; Kasen et al. 2015, etc); assessing the detectability of EM counterparts (Metzger & Berger 2012; Cowperthwaite & Berger 2015); comparing followup capabilities of various facilities (Nissanke et al. 2013; Kasliwal & Nissanke 2014); and strategies for coordination and optimal followup (Singer et al. 2012; Chan et al. 2015; Ghosh et al. 2015; Rana et al. 2016). The search for optical counterparts of GW sources is among the driving scientific interests for upcoming projects like BlackGEM<sup>2</sup> (Bloemen et al. 2015) and the Gravitational-wave Optical Tran-

oranda of understanding with the LIGO–Virgo collaboration is available at [https://gw-astronomy.org/wiki/LV\\_EM/PublicParticipatingGroups](https://gw-astronomy.org/wiki/LV_EM/PublicParticipatingGroups).

<sup>2</sup> BlackGEM — <https://astro.ru.nl/blackgem/>

<sup>1</sup> A partial list of groups which have signed mem-

sient Observer (GOTO<sup>3</sup>).

In this work, we examine another factor that can influence the odds of successful followup: the location of the observatory. GW detectors are not uniformly sensitive to the entire sky, which introduces a sky position dependent bias in the detection and localization of sources (Fairhurst 2011). It is then fair to ask, for instance, if observatories located on the same continent as the two LIGO detectors are “better placed” for the search for electromagnetic counterparts of gravitational wave sources. A second location-related effect comes from the timing of the LIGO science runs. For instance, for an observing run during northern winter would mean that on an average, a larger part of the localization region is visible to northern observatories during the long nights. It is our aim to examine the effects of these two factors on the follow-up capabilities of various observatories (cf. Chen et al. 2016).

We frame our question and describe our methods in §2. We explore the effects of seasons on observing capabilities of various telescopes in §3. We consider the overall effects of geographic location and timing of the LIGO observing runs for two- and three- gravitational wave detector networks in §4, and conclude by discussing the implications in §5.

## 2. METHOD

The principal aim of this work is to investigate the effects of (1) location, and (2) seasons on the probability of finding EM counterparts of GW sources from ground-based observatories.

To undertake these comparisons, we need to disentangle the telescope capabilities from location and seasonal effects. We can phrase the question as follows: “If a telescope based at site  $X$  can cover  $N$  sq. deg. on the sky to the requisite sensitivity in a single night, what would be the probability of it finding the EM counterpart?” We answer this question by simulating follow-up optical/infrared observations of a set fake gravitational wave events from various ground-based locations at various times.

As a representative sample of locations of ground-based observatories, we select all optical/infrared telescopes that participated in the followup of GW150914 (Abbott et al. 2016c). To fill a hole in Asia, we include Hanle (Prabhu 2006), the site of the upcoming 0.7 m robotic telescope, the Indian element of the “Global Relay of Observatories Watching Transients Happen” (GROWTH<sup>4</sup>). The sites considered in

this work are shown in Figure 1, and listed in Table 1.

### 2.1. Simulated GW events

We use gravitational wave events from binary neutron star coalescence simulations by Singer et al. (2014), who used realistic detector sensitivity for LIGO–Hanford (H), LIGO–Livingston (L) and Virgo (V) at various stages of the gravitational wave network to recover the injected events that meet pre-defined detection thresholds. They calculate sky localization of these events using BAYESTAR (Singer & Price 2016), and supply the products as HEALPix files (Gorski et al. 2005). Singer et al. (2014) had simulated detections by LIGO in a period from 18 Aug to 19 Oct for two observing sessions, with gravitational wave detector sensitivity corresponding to the O1 and O2 observing runs. We note that the actual sensitivities attained in LIGO–Virgo observing runs may be somewhat different from their adopted values, thereby altering the localizations to some extent. The final data set<sup>5</sup> contains 630 two-detector events at O1 sensitivity; while for O2 sensitivity it has 365, 15 and 14 events for HL, HV and LV respectively, and 81 three-detector events with O2 sensitivity. Their dates do not match the actual dates of the O1 GW observing run, and are inconsistent with expected dates for O2. Further, the dates may introduce a seasonal bias in the comparison of various locations, as southern observatories will get longer nights in northern summer, and vice versa. Hence, we need to move these simulated events to different dates for comparison.

The sensitivity of LIGO, and hence the localization of detected events, is fixed in geocentric coordinates (Fairhurst 2009). The simulated GW detections can thus be reassigned to any other time when the relative orientations of the geocentric and celestial coordinate systems are the same. Thus, the event localization region in celestial coordinates remains unchanged if any event is moved to the same sidereal time on another day. As a further generalization, events can be moved to an arbitrary time stamp by considering the sky localization in geocentric coordinates, and transferring it to appropriate celestial coordinates at the new time stamp (see for example Evans et al. 2015).

### 2.2. Selection of dates

To disentangle the effects of location and seasons, we first consider an idealized case where all detections are on the dates of the equinoxes, where all sites on earth have the same amount of night time. To evaluate the extent of seasonal variations, we also simulate observa-

<sup>3</sup> GOTO — <http://www.goto-observatory.org/>

<sup>4</sup> GROWTH — <http://growth.caltech.edu>.

<sup>5</sup> The simulated localization files are available at <http://www.ligo.org/scientists/first2years/>.

**Table 1.** Locations of ground-based Optical/IR observatories that followed up GW150914

Site	Telescope/Instrument	Latitude	Longitude	Altitude	Reference	URL
Blenheim, New Zealand	BOOTES-3	45°S	169°41'E	27 m	Castro-Tirado et al. (2012)	<a href="http://bootes.iaa.es/en/">http://bootes.iaa.es/en/</a>
Mt. Siding Spring, Australia	Skymapper	31°16'S	149°04'E	1163 m	Keller et al. (2013)	<a href="https://en.wikipedia.org/wiki/Siding_Spring_Observatory">https://en.wikipedia.org/wiki/Siding_Spring_Observatory</a>
Sutherland, South Africa	MASTER-SAO	32°17'S	20°18'E	1760 m	Lipunov et al. (2010)	<a href="http://observ.pereplet.ru">http://observ.pereplet.ru</a>
La Serena, Chile	DECam (CTIO)	30°10'S	70°48'W	2207 m	Abbott et al. (2012)	<a href="http://www.ctio.noao.edu/noao/">http://www.ctio.noao.edu/noao/</a>
La Silla, Chile	TAROT-LaSilla	29°15'S	70°43'W	2400 m	Boër et al. (1999)	<a href="http://tarot.obs-hp.fr/infos/">http://tarot.obs-hp.fr/infos/</a>
Cerro Paranal, Chile	VST	24°37'S	70°24'W	2600 m	Capaccioli & Schipani (2011)	<a href="http://www.eso.org/public/teles-instr/">http://www.eso.org/public/teles-instr/</a>
Salta, Argentina	TOROS	24°36'S	67°19'W	4650 m	Diaz et al. (2014)	<a href="http://toros.phys.utb.edu/">http://toros.phys.utb.edu/</a>
Mauna Kea, Hawaii	W. M. Keck	19°49'N	155°28'W	4145 m	Faber et al. (2003)	<a href="http://www.keckobservatory.org/about/">http://www.keckobservatory.org/about/</a>
Haleakala, Hawaii	PanSTARRS	20°42'N	156°15'W	3052 m	Kaiser et al. (2010)	<a href="http://neo.jpl.nasa.gov/programs/">http://neo.jpl.nasa.gov/programs/</a>
Canary Islands, Spain	Liverpool	28°45'N	17°52'W	2363 m	Steele et al. (2004)	<a href="http://telescope.livjm.ac.uk/About/">http://telescope.livjm.ac.uk/About/</a>
Hanle, India	Hanle	32°47'N	78°52'E	4500 m	Prabhu (2006)	<a href="http://www.iiap.res.in/iaa_site">http://www.iiap.res.in/iaa_site</a>
Palomar, USA	PTF	33°21'N	116°51'W	1712 m	Law et al. (2009)	<a href="https://en.wikipedia.org/wiki/Palomar_Mountain">https://en.wikipedia.org/wiki/Palomar_Mountain</a>
Mt. Ontake, Japan	Kiso	35°47'N	137°37'E	1130 m	Takase et al. (1977)	<a href="http://www.ioa.s.u-tokyo.ac.jp/kisohp/TELS/teles_e.html">http://www.ioa.s.u-tokyo.ac.jp/kisohp/TELS/teles_e.html</a>

NOTE—See Figure 1 for a plot of these locations.

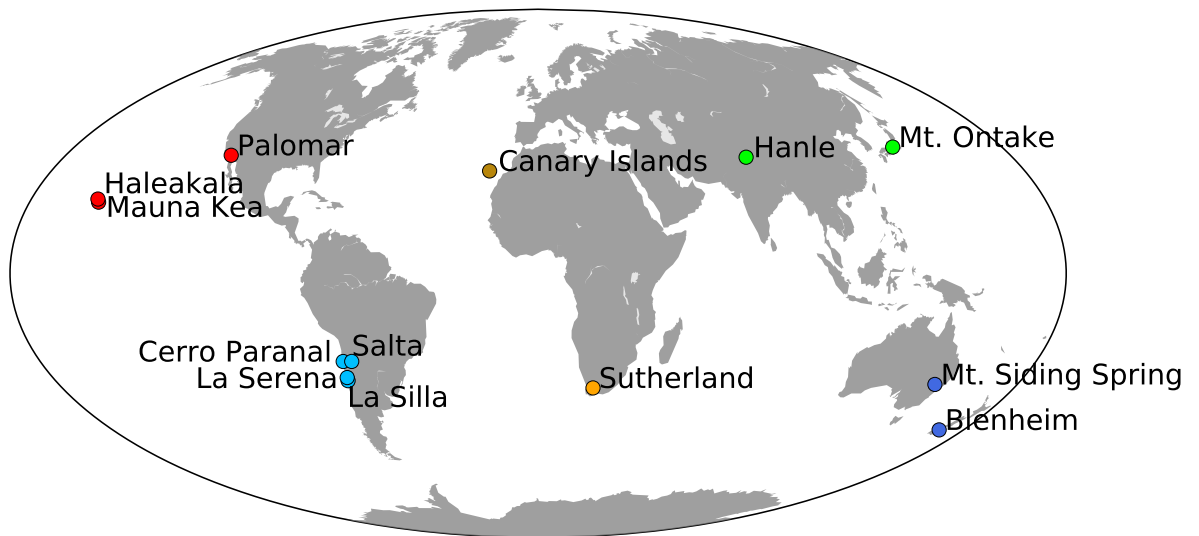


**Figure 1.** Locations of observatories that are considered in this work. We include all ground-based optical/infrared observatories that were involved in following up GW150914. We also include Hanle as a representative observatory in Asia.

tions for cases where all events occur at the summer or winter solstice. These cases are discussed in detail in §3.

Next, in §4 we consider a set of dates for the first and second LIGO–Virgo observing runs, O1 and O2. For O1, we use the actual dates: 18 Sep 2015<sup>6</sup> to 12 Jan 2016<sup>7</sup>. For O2, we consider specific possible dates to allow our analysis to be performed, and the likely split into two parts. We consider O2A, with Hanford and Livingston detectors, to span the period from 1 Dec 2016 to 28 Feb 2017. For our example, Virgo is taken to join these two detectors in O2B, spanning the period from 1 Apr 2017 to 31 May 2017. Considering that not all detectors will be functioning throughout these phases, we undertake separate analysis of O2B into two–detector events (§4.1) and three–detector events (§4.2).

### 2.3. Analysis

We load and analyze the HEALPix files in python using `healpy` and `astropy` (Robitaille et al. 2013). We consider the 99% credible region for GW localization, and hereafter refer to it as a “patch”. Observations are simulated for a period of 24 hours from the trigger, and limited to night time (sun at least 18° below the horizon). We also impose an upper bound on the zenith angle of observations, based on two principles: most telescopes cannot point arbitrarily close to the horizon, and quality of data is poor for observations at high airmass<sup>8</sup> (high zenith angle). We choose an airmass of  $\sim 2.5$ , so that only parts of the patch that rise at least 24° above the horizon are observed. We do not include any constraints based on lunar phase or lunar angle.

After filtering out the HEALPix pixels satisfying these conditions, we sort them by probability of containing the EM counterpart, and add up the probability for the top  $N$  sq. deg.. To enable comparisons with real telescopes, we have considered different cases with  $N = 1, 3, 10, 30, 100$  and 300 sq. deg.

For reference, we also consider a best-case scenario that could be attained by say a space telescope, free of horizon and twilight constraints. In this case, we only mask out pixels within a 42° sun avoidance angle<sup>9</sup>. This case is marked as “best” in the following sections.

We note two important caveats in these analyses: we have not considered the shape of a telescope field of view, or the duration of visibility of the patch. For instance, if

a patch is irregularly shaped, each telescope image may include several parts of the sky that are outside the 99% patch (cf. Ghosh et al. 2015). Thus, the telescope may image say 100 sq. deg., but cover only 50 sq. deg. of our patch. This inefficiency is sensitive to the exact shape and size of the field of view. There might also be scenarios where a large part of the patch is visible from the site, but only for a short duration of time: for instance, an event occurring overhead just before morning twilight. However, the time taken to image  $N$  sq. deg. to a given depth can vary drastically between different telescopes. This in turn may limit the fraction of the visible patch that can be imaged through the night. As our focus is to compare geographic locations rather than telescopes and instruments, we do not consider these two effects in our simulations.

## 3. GEOGRAPHICAL AND SEASONAL EFFECTS AT SOLSTICES AND EQUINOXES

As discussed in §2.2, we first compare the various observatory locations in terms of their coverage for GW events on equinoxes. First, consider the case of all 1024 (O1 + O2) two-detector events moved to the Autumnal equinox. For each event, we calculate the probability observable from each location, and find that all sites have comparable performance. As an example, in Figure 2 we show histograms of the probability of finding the counterpart by imaging the best visible 30 sq. deg. from two sites — Blenheim, New Zealand and Haleakala, Hawaii — which respectively had the worst and best median performance in this category. It is seen that both sites have a comparable performance.

In order to simplify visual comparisons, in the rest of this paper we use box-and-whisker plots (Figure 2, lower panel). The filled box spans the central 50% of the histogram, extending from the lower quartile to upper quartile. In other words, 25% of the events have observable probability less than the left edge of the box, while it is greater than the right edge for another 25%. The range between these two points is called the interquartile range (IQR). “Whiskers” plotted on either side of the box extend to  $1.5 \times \text{IQR}$ <sup>10</sup>. Any outlier points outside the whiskers are marked by red ‘+’ signs. Since we are primarily interested in properties of the distribution rather than specific outliers, we have often scaled the plots such that some of the outliers are beyond the plot limits. The line and star inside the box show the median and mean of the distribution.

Next, we investigate the effect of seasons by simulating observations of the same 1024 (O1 + O2) two-detector

<sup>6</sup> O1 start date: [www.ligo.caltech.edu/news/ligo20150918](http://www.ligo.caltech.edu/news/ligo20150918).

<sup>7</sup> O1 end date: [www.ligo.caltech.edu/news/ligo20160112](http://www.ligo.caltech.edu/news/ligo20160112).

<sup>8</sup> Airmass is the relative optical path length for light through the Earth’s atmosphere, and is set to unity for a source exactly overhead.

<sup>9</sup> As we have selected 18° twilight and a 24° altitude constraint, any observatory anywhere in the world will not be able to observe any point  $< 42^\circ$  from the sun.

<sup>10</sup> If the histograms were Gaussian, the ends of the whiskers would be at  $4.7\sigma$  on either side of the mean.

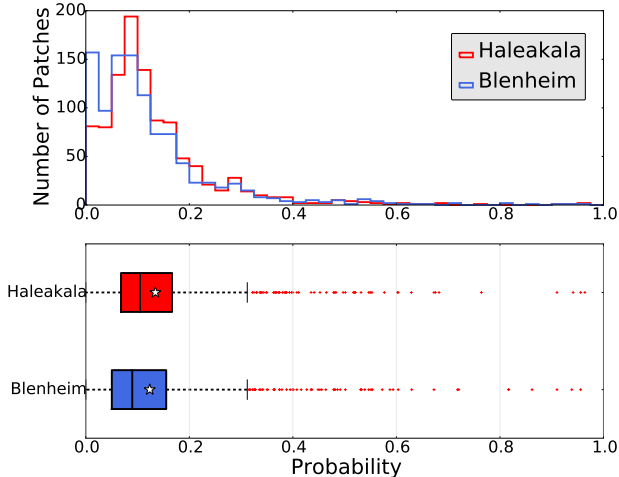


**Figure 2.** Comparing the observable probabilities for Blenheim and Haleakala, sites of BOOTES3 and PanSTARRS respectively. We simulated observations of 1024 GW events detected by the two-detector network (O1 or O2), with all events moved to the date of the autumnal equinox. We assume that each site has a telescope capable of imaging 30 sq. deg. to the requisite sensitivity. The overall histograms are comparable. The slightly poorer observability from Blenheim results from a greater distance from the equator, which makes some northern patches completely inaccessible. *Upper panel:* Histograms of observable probabilities for all events. *Lower panel:* Box and whisker plots for the same histograms.

patches, but moved to the dates of the solstices. As expected, we see that northern observatories perform better during the winter solstice, owing to longer nights; while southern observatories perform better during the summer solstice. For example, Figure 3 shows the performance of La Serena, Hanle, and Palomar Mountain on the equinoxes and solstices, showing clearly the reversal of favored seasons between the northern and southern hemispheres.

While the overall performance of the various sites for equinox observations is similar (Figure 4), looking at the median values of observable probabilities shows some interesting trends (Figure 5). We see that on the equinoxes, sites at mid-latitudes have a few percent higher probability of finding the optical counterpart of a gravitational wave event, as compared to observatories in the temperate zones. This can be explained by a combination of two effects: (i) the two LIGO detectors detect more sources at mid-declinations as compared to equatorial or polar declinations, and (ii) sites further from the equator have a progressively smaller fraction of the sky accessible even on the equinox night. Similar effects have also been discussed in Chen et al. (2016).

We also see that if we cover 100 sq. deg. of the sky from any given location, the median observable proba-

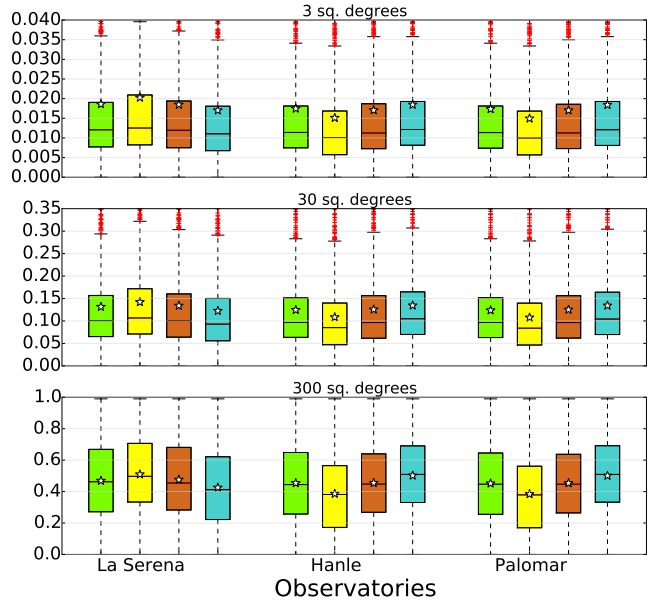


**Figure 3.** Location-wise performance comparison between La Serena, Hanle, and Palomar, for all the O1 and O2 two-detector events. Events were shifted to the day of vernal equinox (green), summer solstice (yellow), autumn equinox (chocolate) and winter equinox (blue). The three panels distribution of observable probabilities are calculated using telescopes that can image 3, 30 and 300 sq. deg. respectively within 24 hours of the trigger.

bility for events on the day of the solstice changes by 1% to 7% with respect to equinox, and these differences are stronger for sites further away from the equator (Figure 5, upper panel). This seasonal variation stems primarily from the duration of the night, determining the fraction of the sky visible. The effect is limited to a few percent due to the large areas and long arc-like shapes of GW events localized by just two detectors (Singer et al. 2014). One would then expect the seasonal differences to be more stark if the localization improves. In the limiting case, if GW sources were pinpointed on the sky by the gravitational wave detectors, the observable probability would be governed by the latitudinal variation of detector sensitivity function (Fairhurst 2011) and would vary more strongly with the fraction of the sky visible at night. Indeed, this is the case with improved localizations provided by a network of three gravitational wave detectors. We repeat our simulations using GW events that were detected by the HLV network, and find that solstice-to-solstice changes in the median observable probability can be as high as 60% (Figure 5, lower panel). For reasons discussed in §4.2, results for the three-detector network should only be considered qualitatively, not quantitatively.



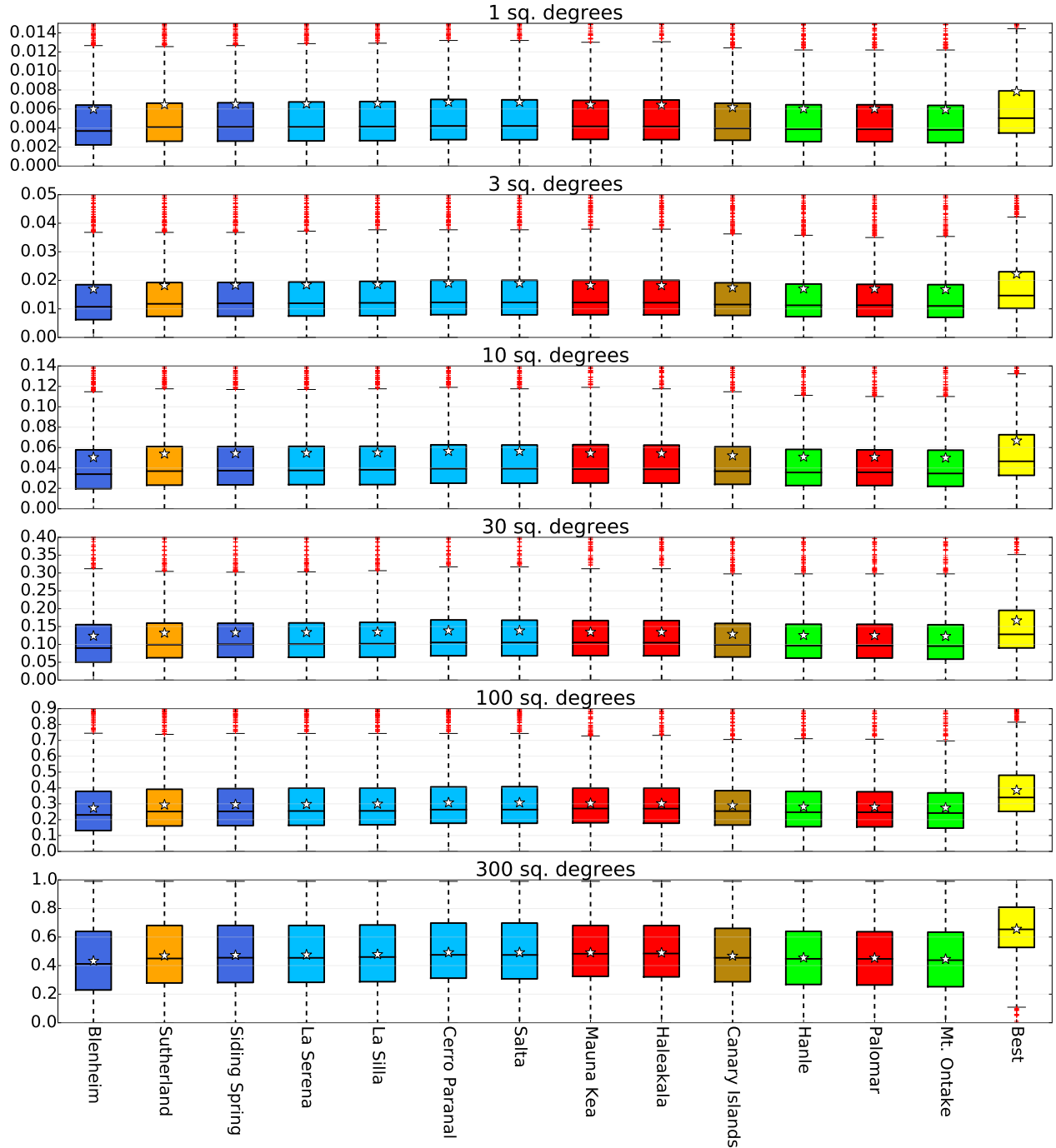


**Figure 4.** Probability of finding optical counterparts for simulated two-detector events on the autumnal equinox. The simulation sample includes events with O1 and O2 sensitivity. The observatories are sorted by longitude, and color-coded by continent as in Figure 1. The best-case scenario considering only solar exclusion angle but ignoring horizon constraints is plotted in the rightmost column. On comparing the location-wise performance for 1, 3, 10, 30, 100 and 300 sq. deg., we see that all sites perform comparably with a very slight trend along the latitude.

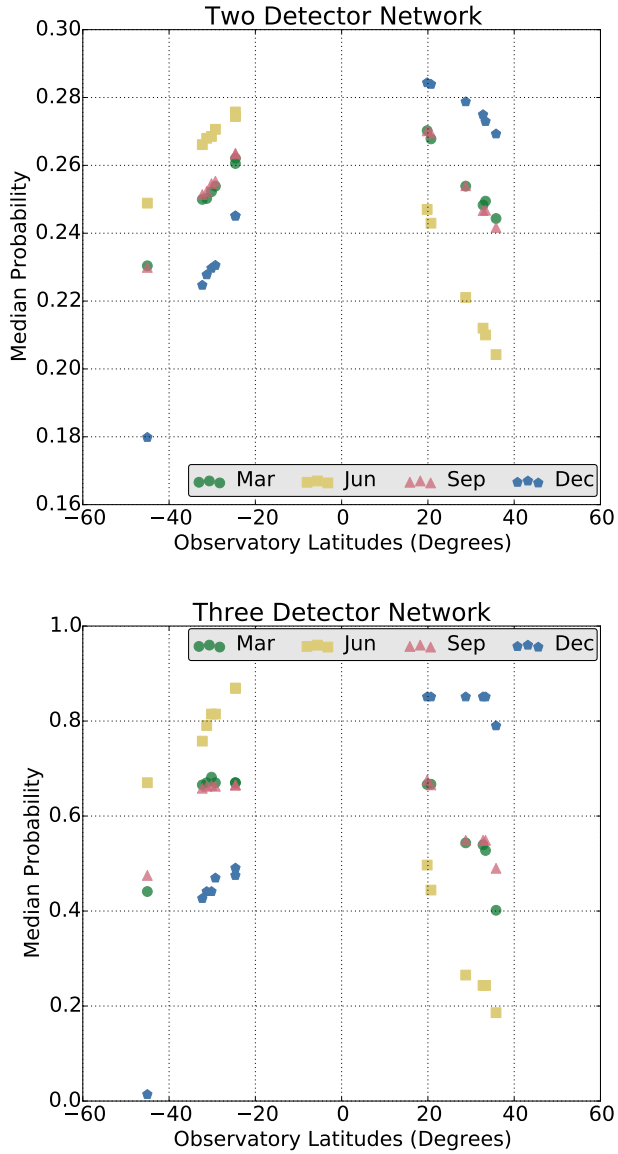


**Figure 5.** Effects of seasons on median observable probability for different latitudes. The different colors and symbols show median observable probability on the days of the vernal equinox (green circles), summer solstice (yellow squares), autumnal equinox (pink triangles) and winter solstice (blue pentagons). *Upper panel:* For each site, we compute the median of the probability covered for 1024 (O1 + O2) two detector events, with a telescope limited to observing 100 sq. deg. during the night. *Lower panel:* Median probability of finding the counterpart for a source localized by a the three detector HLV network, with the same telescopes limited to observing 100 sq. deg. during the night.

#### 4. EXAMPLE OBSERVING RUNS

As a specific case, we repeat our simulations using the actual dates of the first LIGO science run (O1) and a set of example dates of O2. Although the dates of O2 are uncertain, we aim to give an overall perspective of how observatories at different locations may perform under

these conditions. The qualitative nature of these results will be insensitive to  $\sim 10$  day shifts in dates.

##### 4.1. Two Detector Network

Our two-detector sample consists of 630 events with O1 sensitivity, and 394 events at O2 sensitivity. The latter are split as 365, 15 and 14 events for HL, HV and LV respectively. The relatively smaller number of Virgo-detected events arises from expected sensitivity and uptime of the three detectors, as discussed in [Singer et al. \(2014\)](#). As discussed in §2.2, O2 is expected to be subdivided into O2A and O2B. For our simulations, we distribute the 365 HL events randomly in both parts of the run, and keep the 29 HV/LV events in O2B.

As O1 was conducted during northern winter, one expects northern observatories to perform better than southern ones, and this expectation is borne out by simulations (Figure 6). Mauna Kea and Haleakala have the best chance of discovering an optical counterpart, with a median probability of 0.30 for a camera capable of imaging 100 sq. deg. in a night. Blenheim, the southernmost location in this study, had a median probability of 0.22 of imaging the optical counterpart with the same resources. Incidentally, the localization of GW150914 happened to peak in the southern skies ([Abbott et al. 2016a](#)), while localizations of GW151226 and LVT151012 were more uniformly spread over declination ([The LIGO Scientific Collaboration & the Virgo Collaboration 2016](#)). Thus, small number statistics worked in favor of southern observatories in O1.

The assumed split dates of O2 span approximately northern winter and spring, slightly favoring northern observatories in O2A and southern ones in O2B. The net result is that the timing of observing runs slightly favors northern observatories, but the overall performance of observatories is dominated by their latitude, following a similar trend as the equinoxes (Figure 7). The number of two-detector detections involving Virgo in O2B is rather small, and does not alter the trends in any significant manner.

##### 4.2. Three Detector Network: HLV

The joint detection of any gravitational wave event by all three GW detectors drastically changes the follow-up scenario. The median area encompassing 90% probability of containing the true source drops from several hundreds of square degrees to few tens of square degrees ([Singer et al. 2014](#)). We now investigate how this affects the follow-up from various locations.

[Singer et al. \(2014\)](#) provide only 81 events detected by the HLV network. As the net area of each localization patch is a small fraction of the entire sky, any study using this sample will suffer from small number statistics. Indeed, averaging the all-sky probabilities for



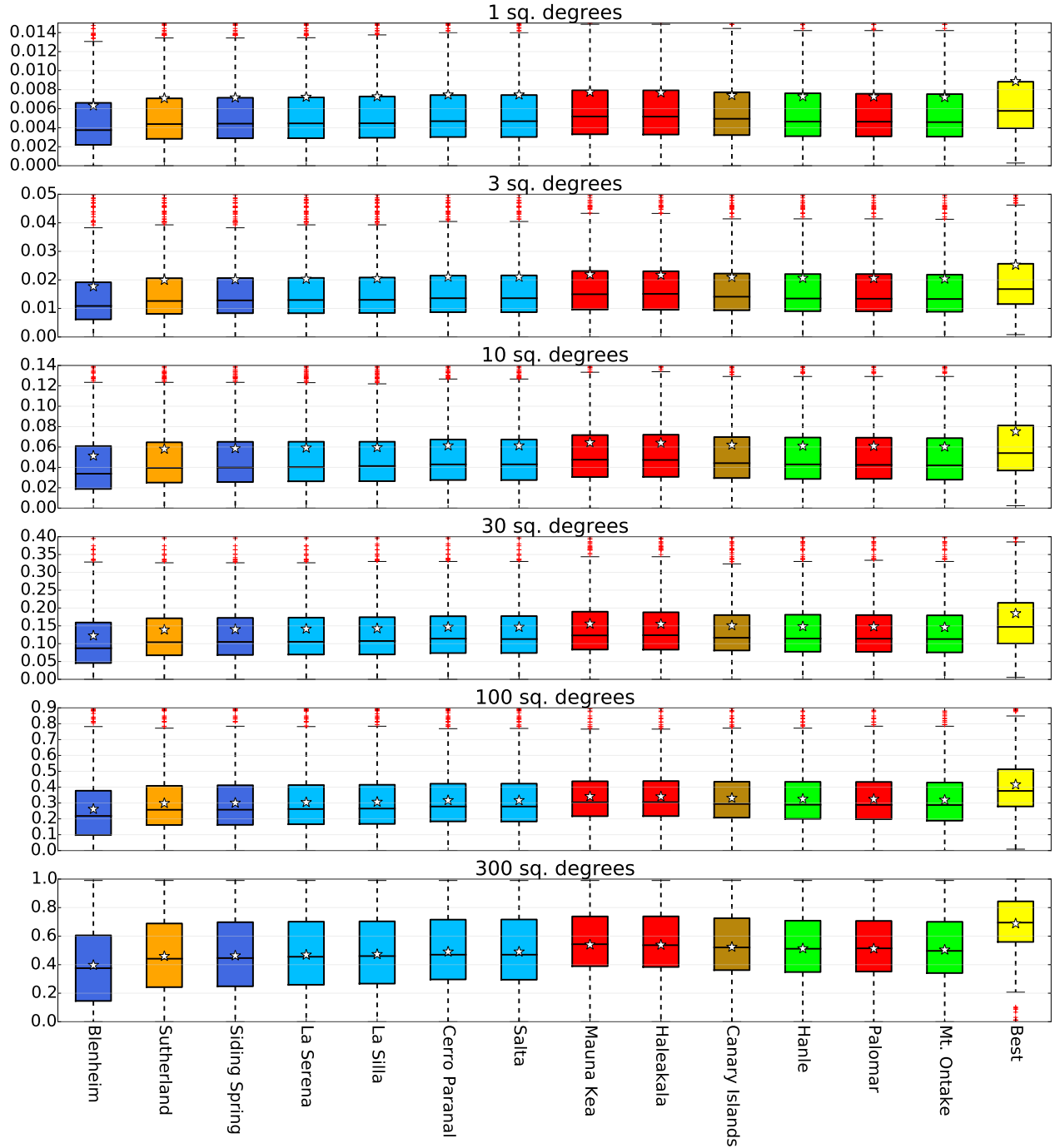


**Figure 6.** Comparisons of various observatories for O1. 630 simulated events detected with Hanford and Livingston GW detectors at O1 sensitivity were randomly distributed over actual dates of O1. The box-plots of observable probabilities are as in Figure 4. Northern observatories had better chances of finding EM counterparts as compared to southern ones.

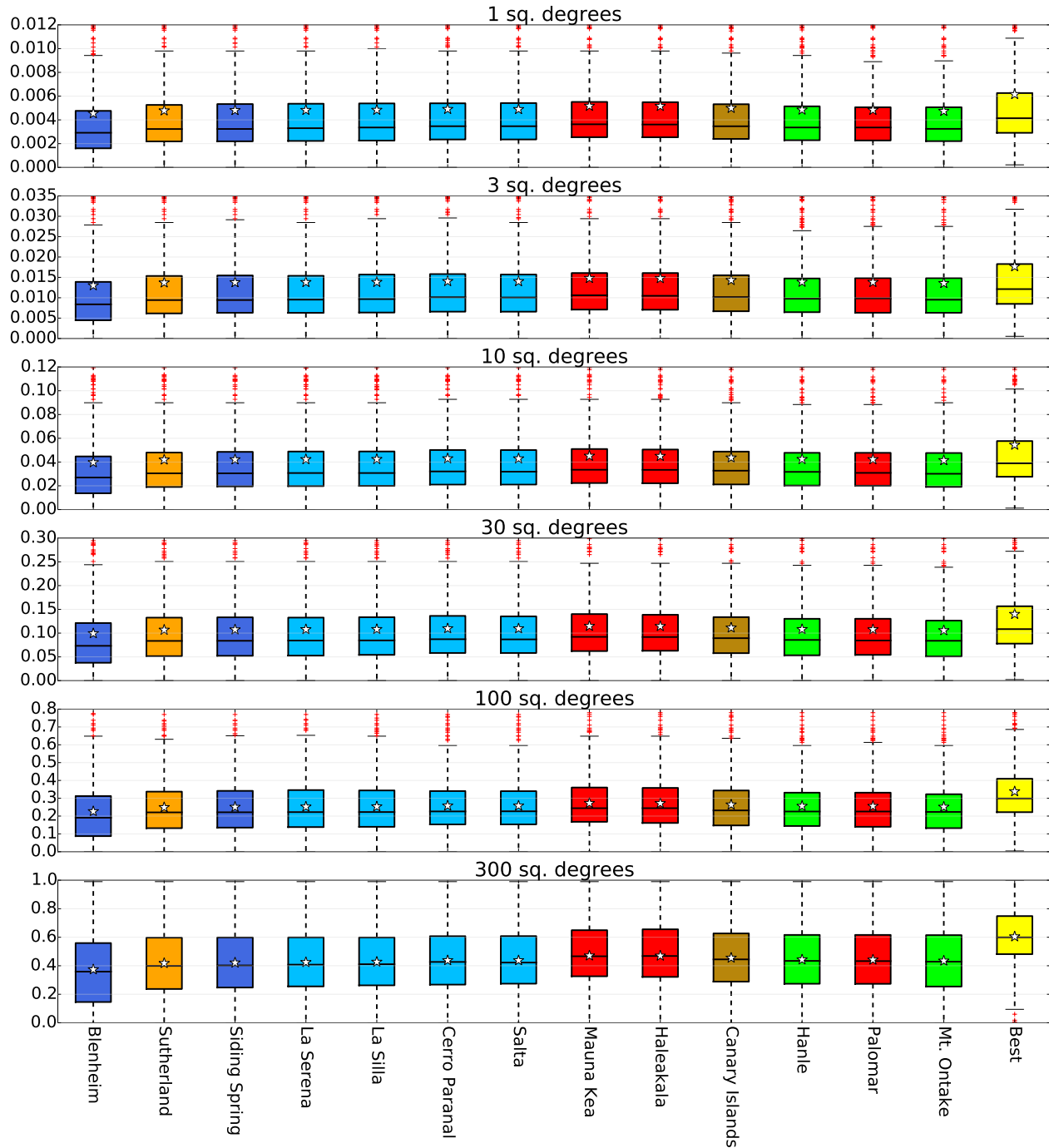


**Figure 7.** Comparisons of various observatories for O2. 394 simulated events detected with GW detectors at O2 sensitivity were distributed over example dates of O2 as described in §4.2. The box-plots of observable probabilities are as in Figure 4. Operational periods O2A and O2B favor locations in different hemispheres, as a result, all observatories have comparable odds of finding EM counterparts of GW sources.

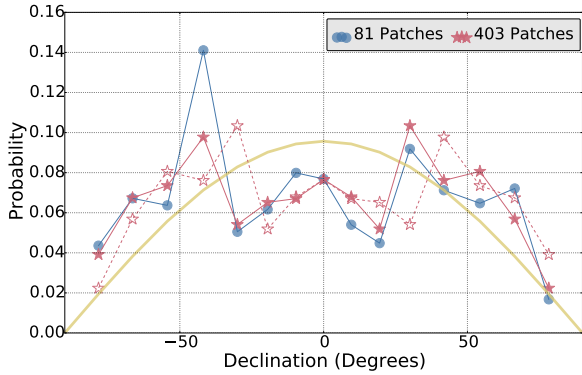


**Figure 8.** Probability of source location as a function of declination, averaged over multiple patches. The solid yellow curve is proportional to  $\cos(\delta)$ , the expected probability distribution if the sensitivity of gravitational wave detectors was independent of direction. Blue circles show the distribution for the average of the original 81 patches from [Singer et al. \(2014\)](#), with a strong peak at  $\delta \sim -40^\circ$ . Solid brown stars show the average probability in each declination bin for the average of the final 403 patches used in this work. To guide the eye, hollow brown stars connected with dashed lines show a mirror image of the final probability distribution: showing that the final set has reasonable north-south symmetry.

these 81 events shows a bias towards the southern skies (Figure 8, blue circles). We work around this problem in two steps. First, we translate these patches in trigger times (and right ascensions) to get 400 new sky localizations as discussed in §2.1. Next, we randomly select 20% of the patches with localization peaking in the southern hemisphere, and drop them from the set. This nearly removes the unexpected north-south asymmetry in the full sample (Figure 8, brown stars). This gives us a final set of 403 patches, which we distribute randomly over the dates of O2B for simulating followup of three-detector events.

The well-constrained sky localizations from the three detector network lead to very different distributions of observable probability as compared to a two detector network. Observatories at most locations can cover nearly the entire patch if it rises at that location, but cover almost zero probability otherwise. Figure 9 highlights this effect for telescopes that can cover 30 sq. deg. in a single night. At all observatories, a large fraction of events have  $p_{\text{obs}} < 0.05$  or  $p_{\text{obs}} > 0.95$ . The overall result is that the observable probability from any given location (Figure 10) is completely dominated by seasonal effects. For the dates of O2B used in this work, our simulations show the southern locations stand a better chance of finding optical counterparts of gravitational wave sources. As the 403 patches used in these simulations were generated from just 81 events, we caution the reader that these results should be interpreted qualita-

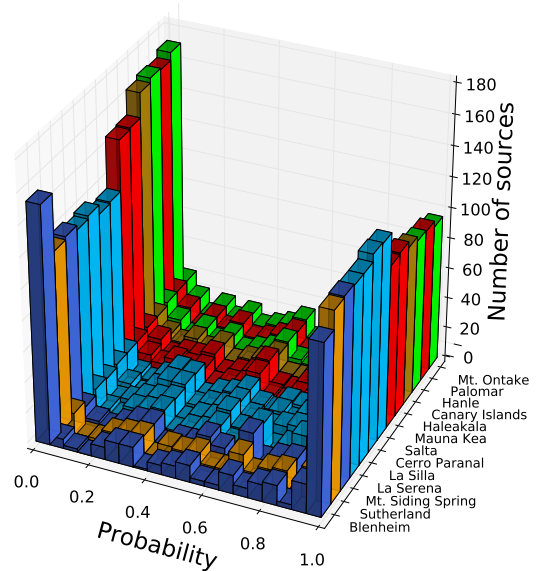


**Figure 9.** Probability of imaging the counterpart of a gravitational wave event from various locations for the 403 events recovered with a three gravitational wave detector network. We have assumed that instruments at each location can observe 30 sq. deg. of the sky. As many events have rather small 99% localization areas, observations will be dominated by whether the localization region is visible at all. A large fraction of events have  $p_{\text{obs}} < 0.05$  or  $p_{\text{obs}} > 0.95$ .

tively.

## 5. DISCUSSION

We investigate the effects of observatory locations on the probability of discovering optical/infrared counterparts of gravitational wave sources. We show that the odds of discovering EM counterparts show some latitude dependence, but weak or no longitudinal dependence.

Seasons have a much larger effect on the observability of GW localization regions, and dominate over geographic variations. These effects too are stronger for observatories at high latitudes, where the length of the night is most strongly affected by seasons. [Chen et al. \(2016\)](#) have independently reached similar conclusions by using a different methodology and slightly different assumptions.

Our simulations show that northern observatories had slightly better odds of discovering the EM counterparts of GW sources in O1, though the small number statistics of just two detections and one candidate dominated over this effect. Based on our assumed sample dates of the second observing run O2, all observatory locations have comparable chances of finding EM counterparts.

In mid-2017, O2B may discover the first three-detector GW event, with much better localization than two-

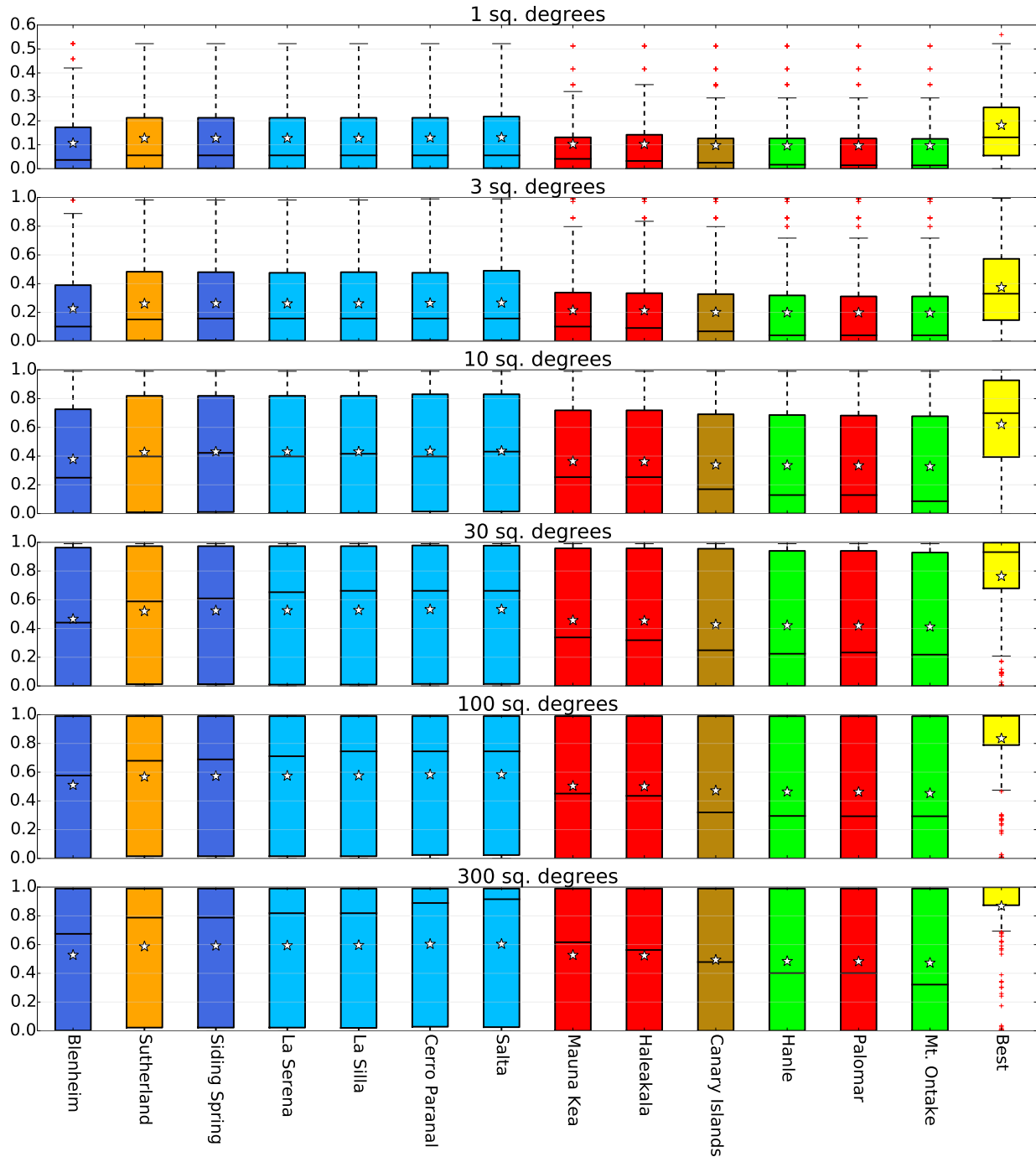


**Figure 10.** Probability of finding optical counterparts for simulated three-detector events with example O2B dates. Details are as in Figure 4. While box-plots are not the best representations of these bi-peaked distributions (see Figure 9), we use them for consistency with other plots. The better performance of southern locations can be attributed primarily to the season. As we increase the sky coverage, the mean probability of finding a counterpart increases rather slowly beyond  $30^\circ$ .

detector networks: simplifying ground-based follow-up. This season favors southern observatories, giving them significantly higher chances of discovering counterparts of such GW events.

In order to compare the performance of various optical/infrared observatory sites, we have assumed identical equipment at all locations. In practice, this is not the case and instrument characteristics like imaging depth and field of view will play a strong role in successful detection of an EM counterpart. Coordinated observations among multiple sites (Singer et al. 2012), use of galaxy catalogs (Hanna et al. 2014; Gehrels et al. 2015) and enhanced scheduling algorithms (Chan et al. 2015; Ghosh et al. 2015; Rana et al. 2016) will help observatories to boost their chances of detecting electromagnetic counterparts.

We have taken a representative sample of observatories and considered a set of example dates of LIGO–Virgo observing runs for our simulations. To facilitate further exploration on these lines, our simulation codes are available at <https://github.com/emvarun/followup-and-location>. Users will also have to download the Singer et al. (2014) data set from <http://www.ligo.org/scientists/first2years/>. In these python codes, users can easily add/remove sites and change simulation dates. The codes produce a set of plots, summary tables, and a detailed table for the observable probability of each event from each location.

## ACKNOWLEDGMENTS

We thank P. Ajith, Hsin-Yu Chen, Reed Essick, Shaon Ghosh, N. K. Johnson-McDaniel and Leo Singer for helpful discussions.

VB acknowledges the financial support of Department of Science and Technology, Government of India for the “Global Relay of Observatories Watching Transients Happen (GROWTH)” project which prompted this study. GROWTH is a part of “Partnerships for International Research and Education (PIRE)”, jointly funded by NSF grant No. 1545949. APR acknowledges the ICTS-S. N. Bhatt Memorial Excellence Fellowship Program for his summer at ICTS during which a large initial part of the work was done. AG’s research was supported by the AIRBUS Group Corporate Foundation Chair in “Mathematics of Complex Systems” at ICTS, and by the Max Planck Society and the Department of Science and Technology, Government of India, through a Max Planck Partner Group at ICTS. SB acknowledges support from NSF grant PHY-1506497.

This LIGO document P1600278-v2.

*Software:* NumPy (van der Walt et al. 2011) and Matplotlib (Hunter 2007), Astropy (Robitaille et al. 2013, <http://www.astropy.org>), HEALPix (Gorski et al. 2005), Healpy (<https://healpy.readthedocs.org/>), Ephem (<https://pypi.python.org/pypi/pyephem/>).

## REFERENCES

- Abbott, B. P., Abbott, R., Abbott, T. D., et al. 2016a, The Astrophysical Journal Letters, 826, L13
- . 2016b, Physical Review Letters, 116, 061102
- . 2016c, The Astrophysical Journal Supplement Series, Volume 225, Issue 1, article id. 8, pp. (2016)., 225, 8
- Abbott, T. M., Muñoz, F., Walker, A. R., et al. 2012, in Ground-based and Airborne Telescopes IV, ed. L. M. Stepp, R. Gilmozzi, & H. J. Hall (International Society for Optics and Photonics), 844445
- Bloemen, S., Groot, P., Nelemans, G., & Klein-Wolt, M. 2015, Astronomical Society of the Pacific Conference Series, 496, 254
- Boër, M., Bringer, M., Klotz, A., et al. 1999, Astronomy and Astrophysics Supplement Series, 138, 579
- Capaccioli, M., & Schipani, P. 2011, The Messenger, 146, 2
- Castro-Tirado, A. J., Jelínek, M., Gorosabel, J., et al. 2012, in Astronomical Society of India Conference Series, Vol. 7, 313–320
- Chan, M. L., Hu, Y.-M., Messenger, C., Hendry, M., & Heng, I. S. 2015
- Chen, H.-Y., Essick, R., Vitale, S., Holz, D. E., & Katsavounidis, E. 2016, ArXiv e-prints, arXiv:1608.00164
- Connaughton, V., Burns, E., Goldstein, A., et al. 2016, The Astrophysical Journal Letters, 826, L6
- Cowperthwaite, P. S., & Berger, E. 2015, The Astrophysical Journal, 814, 25
- Diaz, M. C., Benacquista, M., Belczynski, K., et al. 2014, in The Third Hot-wiring the Transient Universe Workshop (HTU-III), ed. P. W. et Al., Santa Fe, New Mexico, 225–229
- Evans, P. A., Osborne, J. P., Kennea, J. A., et al. 2015, Monthly Notices of the Royal Astronomical Society, 455, 1522
- Faber, S. M., Phillips, A. C., Kibrick, R. I., et al. 2003, in Instrument Design and Performance for Optical/Infrared Ground-based Telescopes, Proceedings of the SPIE, ed. M. Iye & A. F. M. Moorwood, Vol. 4841, 1657–1669
- Fairhurst, S. 2009, New Journal of Physics, 11, 123006
- . 2011, Classical and Quantum Gravity, 28, 105021
- Gehrels, N., Cannizzo, J. K., Kanner, J., et al. 2015, The Astrophysical Journal, 820, 136
- Ghosh, S., Bloemen, S., Nelemans, G., Groot, P. J., & Price, L. R. 2015, Astronomy & Astrophysics, 592, 82
- Gorski, K. M., Hivon, E., Banday, A. J., et al. 2005, The Astrophysical Journal, 622, 759
- Hanna, C., Mandel, I., & Vousden, W. 2014, The Astrophysical Journal, 784, 8
- Hunter, J. D. 2007, Computing in Science & Engineering, 9, 90
- Kaiser, N., Burgett, W., Chambers, K., et al. 2010, in Ground-based and Airborne Telescopes III, Proceedings of the SPIE, ed. L. M. Stepp, R. Gilmozzi, & H. J. Hall, Vol. 7733, 77330E
- Kasen, D., Fernandez, R., & Metzger, B. D. 2015, Monthly Notices of the Royal Astronomical Society, 450, 1777
- Kasliwal, M. M., & Nissanke, S. 2014, The Astrophysical Journal, 789, L5
- Keller, S. C., Schmidt, B. P., Bessell, M. S., et al. 2013, Publications of the Astronomical Society of Australia, 24, 1

- Law, N. M., Kulkarni, S. R., Dekany, R. G., et al. 2009, Publications of the Astronomical Society of the Pacific, 121, 1395
- Lipunov, V., Kornilov, V., Gorbovskoy, E., et al. 2010, Advances in Astronomy, 2010, 349171
- Metzger, B. D., & Berger, E. 2012, The Astrophysical Journal, 746, 48
- Nissanke, S., Kasliwal, M., & Georgieva, A. 2013, The Astrophysical Journal, 767, 124
- Prabhu, T. 2006, in The 9th Asian-Pacific Regional IAU Meeting, ed. W. Sutantyo, P. Premadi, P. Mahasena, T. Hidayat, & S. Mineshige, 287
- Rana, J., Singhal, A., Gadre, B., Bhalerao, V., & Bose, S. 2016, arXiv eprint, 1603.01689
- Robitaille, T. P., Tollerud, E. J., Greenfield, P., et al. 2013, Astronomy & Astrophysics, 558, A33
- Singer, L., Price, L., & Speranza, A. 2012, ArXiv e-prints, 1204.4510
- Singer, L. P., & Price, L. R. 2016, Physical Review D, 93, 024013
- Singer, L. P., Price, L. R., Farr, B., et al. 2014, The Astrophysical Journal, 795, 105
- Singer, L. P., Kasliwal, M. M., Cenko, S. B., et al. 2015, The Astrophysical Journal, 806, 52
- Steele, I. A., Smith, R. J., Rees, P. C., et al. 2004, in Ground-based Telescopes, Proceedings of the SPIE, ed. J. M. J. Oschmann, Vol. 5489, 679–692
- Takase, B., Ishida, K., Shimizu, M., et al. 1977, Annals of Tokyo Astronomical Observatory, Second Series, 16, 74
- Tanaka, M., & Hotokezaka, K. 2013, The Astrophysical Journal, 775, 113
- The LIGO Scientific Collaboration, & the Virgo Collaboration. 2016, arXiv eprint, 1606.04856
- van der Walt, S., Colbert, S. C., & Varoquaux, G. 2011, Computing in Science & Engineering, 13, 22